AIMETA 2017
XXIII Conference
The Italian Association of Theoretical and Applied Mechanics
Luigi Ascione, Valentino Berardi, Luciano Feo, Fernando Fraternali and Antonio Michele Tralli (eds.)
Salerno, Italy, 4–7 September 2017

A MICRO-MACRO HOMOGENIZATION FOR MODELING THE MASONRY OUT-OF-PLANE RESPONSE

D. Addessi[1], **E. Sacco**[2], **and P. Di Re**[1]

[1]Department of Structural and Geotechnical Engineering, Sapienza University of Rome
Via Eudossiana 18, 00184 Rome, Italy
e-mail: {daniela.addessi, paolo.dire}@uniroma1.it

[2] Department of Civil and Mechanical Engineering, University of Cassino and Southern Lazio
Via G. Di Biasio 43, 03043 Cassino, Italy
e-mail: sacco@unicas.it

Keywords: masonry, multi-scale, homogenization, damage, friction.

Abstract. *This study introduces a finite element model based on a two-scale beam-to-beam homogenization procedure for the analysis of masonry structural members undergoing prevailing axial and bending stress states. The model is developed considering the periodic repetition of bricks and mortar joints in regular stack bond arrangement and assuming a linear elastic behavior for the former and a nonlinear response for the latter. At the microscopic heterogeneous scale, the behavior of a Unit Cell (UC) made of a single brick and mortar layer is described through an equivalent Timoshenko beam representation, where a nonlocal damage formulation with friction plasticity governs the mortar nonlinear constitutive relationship. Basing on a semi-analytical approach, the microscopic quantities are, then, homogenized to define an equivalent beam model at the macroscopic scale.*

The proposed finite element model is implemented in standard numerical codes to investigate the response of typical one-dimensional (1D) masonry elements. This study shows the numerical simulation of two experimental tests: a rectangular wallette under out-of-plane bending and a circular arch under vertical forces. The results obtained for the proposed model are compared with those resulting from micromechanical approaches and the experimental outcomes.

1 INTRODUCTION

Past and recent seismic events have shown that collapse of masonry buildings is frequently related to the onset of flexural and shear mechanisms. Hence, the development of efficient numerical procedures to analyze and predict the response of masonry walls is a relevant and interesting task. As known, among the different approaches for modeling masonry structural element response [1], the micro-macro models allow to accurately describe the complex non-linear anisotropic behavior of masonry material, accounting for the details of geometry, arrangement and constitutive response of the components. These, also known as multi-scale approaches, are a fair compromise between the detailed geometric and mechanical description of the masonry composite material and the computational efforts. Recently, multi-scale procedures adopting the computational homogenization, where the micro and macro scales exchange information at each iteration of the global solution procedure, have been successfully employed [2, 3] to describe the in-plane response of masonry. Some efforts have also been devoted to develop micro-macro techniques for the out-of-plane behavior, usually analyzing a 3D Unit Cell (UC) at the microscale linked to a shell model at the macro structural level [4]. Both linear and damage-plastic constitutive behavior is adopted. Kirchhoff-Love thin shells [5] have been mainly proposed, although a number of works focusing on the homogenization procedure for thick shells, based on the Mindlin theory [6], has been recently presented.

This study presents a two-scale model for masonry structures subjected to prevailing axial and bending stress states. Masonry structural elements characterized by a stack bond arrangement along a one-dimensional (1D) direction, like for example columns and arches, are analyzed. Regular arrangements are considered, made of the periodic repetition of bricks and mortar joints. Two micromechanical models are also adopted for comparison, separately discretizing bricks and mortar with 1D and two-dimensional (2D) finite elements (FE) [7]. All the models use a nonlocal damage constitutive law with friction plasticity for the mortar joints and a linear elastic relationship for the bricks. In particular, the two-scale approach adopts 1D beam models at both the microscopic heterogeneous material scale, where a UC made of the sequence of a brick and a mortar layer is defined, and the macroscopic structural scale, where an equivalent homogeneous beam is considered. This permits to solve the nonlinear homogenization problem at the micro-level by means of a semi-analytical approach, thanks to the simplified nature of the governing variables and equations and some simplified assumptions on the mortar constitutive response. The displacement field in the UC is composed of an assigned part, expressed as function of the macroscopic beam strain components, and an unknown perturbation, which is due to the heterogeneous nature of the medium. To evaluate the constitutive response of the mortar joints and solve the evolution problem of the damage and plastic variables, a fiber discretization is introduced and the differential equations governing the boundary value problem on the UC are solved by an iterative procedure. The microscopic stress components are, then, homogenized to obtain the macroscopic beam stress resultants at the Gauss point linked to the analyzed UC. The equilibrium equations at the macro-level are solved through a FE solution procedure, adopting the beam force-based formulation, more efficient and accurate than the displacement-based approach and already applied by the authors to masonry modeling [8]. The two-scale procedure has been implemented in the MATLAB code, while the micromechanical models have been introduced in the FEAP FE program [9].

Two numerical applications on a masonry wallette and an arch are presented, comparing the results obtained with the two-scale 1D model with the experimental outcomes and with those evaluated by employing the 1D and 2D micromechanical models.

2 Micromechanics and homogenization of masonry beam

A heterogeneous masonry beam structural element is modeled, made of the regular repetition of bricks and mortar arranged in stack bond, as shown in Figure 1(a). The two-scale procedure presented in [10] is adopted, considering a homogeneous beam at the structural level (Figure 1(b)). The constitutive response at each Gauss integration point is derived via a homogenization procedure applied to the UC at the microscopic scale (Figure 1(c)). The UC is properly selected and analyzed to reproduce the behavior of the overall composite material.

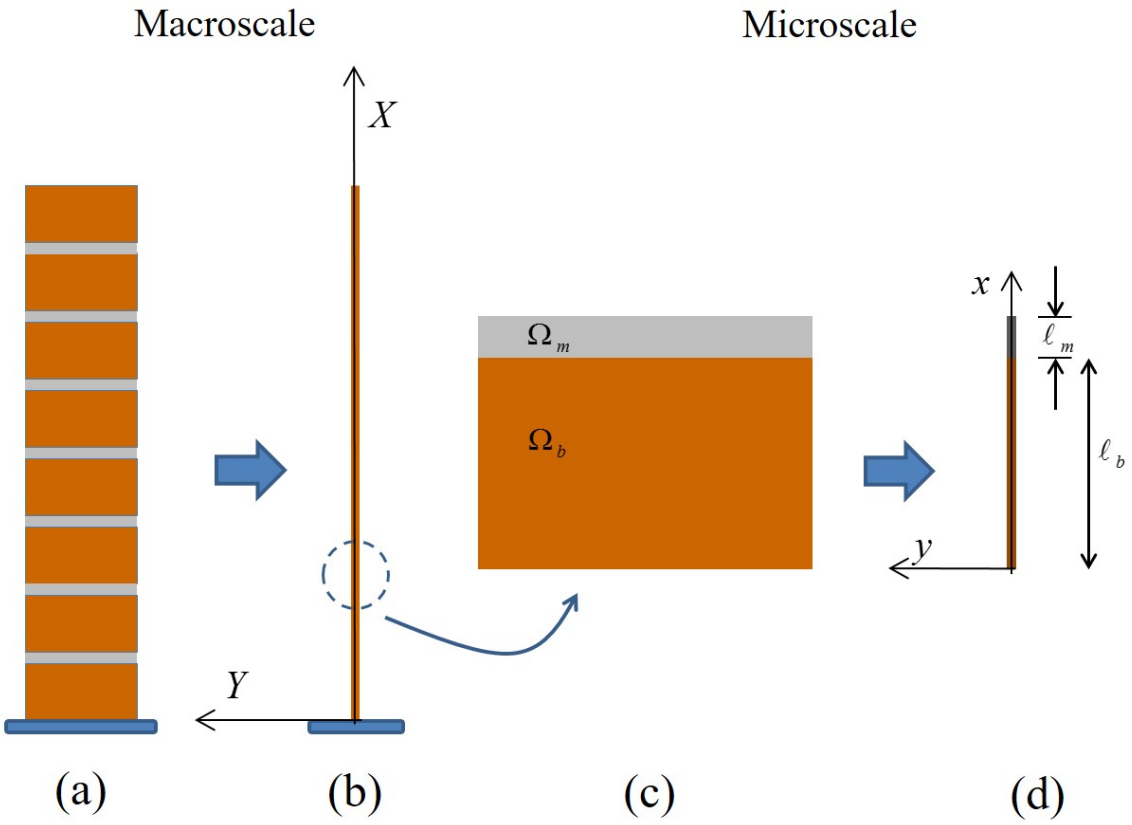

Figure 1: Two-scale analysis of a masonry column: (a) heterogeneous masonry column, (b) homogenized beam model, (c) UC, (d) heterogeneous beam model for the UC.

A beam model is also adopted at the UC scale (Figure 1(d)), and, relying on the rigid section assumption, the displacement components u_1 and u_2 at each point of the beam cross-section are written as:

$$\begin{aligned} u_1 &= u\,(x) - y\,\varphi\,(x) \\ u_2 &= v\,(x)\ , \end{aligned} \tag{1}$$

with u, v and φ representing the generalized displacement components of the beam, i.e. the axial and transverse displacements of the point x, and the rotation of the beam cross-section at x, respectively. The counterclockwise rotation is assumed to be positive.

Considering the periodic texture of the analyzed medium, the displacement components at the microlevel, u, v and φ, are written as the superposition of prescribed fields $\overline{u}$, $\overline{v}$ and $\overline{\varphi}$,

defined as function of the beam generalized strains E, K and Γ, measured at the macroscopic Gauss point, and unknown periodic fluctuations, u^*, v^* and φ^*, satisfying proper periodicity conditions on the UC boundary [11], namely:

$$\begin{array}{rcll} u\left(x\right) & = & \overline{u}\left(x\right)+u^{*}\left(x\right) & \\ v\left(x\right) & = & \overline{v}\left(x\right)+v^{*}\left(x\right) & \text{in} \quad \left(0,\ell\right), \\ \varphi\left(x\right) & = & \overline{\varphi}\left(x\right)+\varphi^{*}\left(x\right) & \end{array} \tag{2}$$

with

$$u^{*}\left(0\right)=u^{*}\left(\ell\right) \qquad v^{*}\left(0\right)=v^{*}\left(\ell\right) \qquad \varphi^{*}\left(0\right)=\varphi^{*}\left(\ell\right) . \tag{3}$$

The prescribed displacement fields $\overline{u}$, $\overline{v}$ and $\overline{\varphi}$ are the solution for the homogeneous UC subjected to the macroscopic strains E, K and Γ, resulting as:

$$\begin{array}{ll} \overline{u}\left(x\right)=E\,x & \\ \overline{v}\left(x\right)=\Gamma\,x+\dfrac{1}{2}K\,x^{2} & \text{in} \quad \left(0,\ell\right). \\ \overline{\varphi}\left(x\right)=K\,x & \end{array} \tag{4}$$

Taking into account formulas (1), (2) and (4), the beam generalized strain parameters, i.e axial strain, curvature and shear strain, are derived as:

$$\begin{array}{rcccl} \varepsilon_0 & = & u' & = & E+u^{*'} \\ \kappa & = & \varphi' & = & K+\varphi^{*'} \\ \gamma & = & v'-\varphi & = & \Gamma+v^{*'}-\varphi^{*} \end{array} \tag{5}$$

where the apex $\cdot'$ denotes the derivative with respect to x.

Enforcing the average conditions, requiring that the generalized strain parameter average values have to be equal to the macroscopic strains, equations (5) lead to:

$$\begin{array}{l} 0=\displaystyle\int_{\ell}\left(u^{*}\right)'\,dx \\ 0=\displaystyle\int_{\ell}\left(\varphi^{*}\right)'\,dx \\ 0=\displaystyle\int_{\ell}\left(v^{*}\right)'\,dx-\int_{\ell}\varphi^{*}\,dx\,. \end{array} \tag{6}$$

which, accounting for the periodicity conditions (3), reduce to the following condition:

$$\int_{\ell}\varphi^{*}\,dx=0\,. \tag{7}$$

The constitutive response of the mortar material is ruled by the following relationships:

$$\begin{array}{rcl} \sigma_m & = & E_m\left(\varepsilon-\pi_{\varepsilon}\right) \\ \tau_m & = & G_m\left(\gamma-\pi_{\gamma}\right), \end{array} \tag{8}$$

where σ_m and τ_m are the normal and shear stresses, ε and γ are the normal and shear strains, π_{ε} and π_{γ} are the normal and shear inelastic strains due to damage, plasticity or other inelastic

effects. Moreover, E_m and G_m denote the mortar Young's and shear elastic moduli. Adopting the constitutive model proposed in [12], it results:

$$\begin{aligned} \pi_\varepsilon &= D\, H\left(\varepsilon\right) \varepsilon \\ \pi_\gamma &= D\, \gamma_p \,, \end{aligned} \tag{9}$$

where D is the damage variable, with $0 \leq D \leq 1$, $H\left(\varepsilon\right) \varepsilon$ reproduces the unilateral effect, being $H\left(\varepsilon\right) = 0$ if $\varepsilon \leq 0$ and $H\left(\varepsilon\right) = 1$ if $\varepsilon > 0$, and γ_p is the shear slip.

To properly account for the fracture modes I and II, the damage evolution is governed by the equivalent strain parameter Y_{eq} and the mode ratio η, defined as:

$$Y_{eq} = \sqrt{\left(\frac{\left\langle \varepsilon \right\rangle_+}{\varepsilon_0}\right)^2 + \left(\frac{\gamma}{\gamma_0}\right)^2} \qquad \eta = \frac{1}{\varepsilon_{eq}^2}\left[\left(\left\langle \varepsilon \right\rangle_+\right)^2 \, \eta_\varepsilon + \gamma^2 \, \eta_\gamma\right] \,, \tag{10}$$

with

$$\eta_\varepsilon = \frac{\varepsilon_0\, \sigma_0}{2\, G_{cI}}, \quad \eta_\gamma = \frac{\gamma_0\, \tau_0}{2\, G_{cII}}, \quad \varepsilon_{eq} = \sqrt{\left(\left\langle \varepsilon \right\rangle_+\right)^2 + \gamma^2} \,, \tag{11}$$

σ_0 and τ_0 being the peak values of the normal and shear stresses, ε_0 and γ_0 the corresponding values of the normal and shear strains, G_{cI} and G_{cII} denoting the fracture energies corresponding to modes I and II and the Macaulay brackets $\left\langle \cdot \right\rangle_+$ evaluating the positive part of the number. The damage is evaluated according to the following law:

$$D = \max_{history}\left\{0, \min\left\{\widetilde{D}, 1\right\}\right\} \qquad \text{with} \quad \widetilde{D} = \frac{Y_{eq} - 1}{\left(1 - \eta\right) Y_{eq}} \,. \tag{12}$$

The Coulomb law rules the evolution of the friction plasticity on the basis of the following yield function:

$$\varphi\left(\widetilde{\sigma}_m, \widetilde{\tau}_m\right) = \mu\, \widetilde{\sigma}_m + \left|\widetilde{\tau}_m\right| \,, \tag{13}$$

where μ is the friction parameter and $\widetilde{\sigma}_m$ and $\widetilde{\tau}_m$ are the normal and shear effective contact stresses, resulting as:

$$\widetilde{\sigma}_m = E_m\left(\varepsilon - H\left(\varepsilon\right) \varepsilon\right) \tag{14}$$

$$\widetilde{\tau}_m = G_m\left(\gamma - \gamma_p\right) \,. \tag{15}$$

The plastic slip evolves according to the evolution equation and the loading-unloading Kuhn-Tucker conditions, expressed as:

$$\dot{\gamma}_p = \dot{\lambda} \frac{\widetilde{\tau}_m}{\left|\widetilde{\tau}_m\right|} \qquad \dot{\lambda} \geq 0 \quad \varphi \leq 0, \quad \dot{\lambda}\, \varphi = 0 \,, \tag{16}$$

where λ is the inelastic multiplier.

Linear elastic constitutive relationships are considered for the brick material, as:

$$\begin{aligned} \sigma_b &= E_b\, \varepsilon \\ \tau_b &= G_b\, \gamma \,, \end{aligned} \tag{17}$$

where σ_b and τ_b are the normal and shear stresses, while E_b and G_b are the Young's and shear elastic moduli in the brick.

By integrating the material stress components (8) and (17) over the mortar and brick cross-section in the UC, the resultant axial force, bending moment and shear force are obtained as:

$$\begin{aligned} n_m &= E_m\, A\, \varepsilon_0 - P & \qquad n_b &= E_b\, A\, \varepsilon_0 \\ m_m &= E_m\, I\, \kappa - R & \qquad m_b &= E_b\, I\, \kappa \\ t_m &= G_m\, A_s \gamma - V & \qquad t_b &= G_b\, A_s \gamma \end{aligned} \tag{18}$$

in the mortar and brick material, respectively. In equations (18), A, I and A_s are the area, the inertia and the shear area of the beam cross-section, respectively. The quantities P, R and V account for the inelastic strains arising in the mortar and result as:

$$P = \int_A E_m\, \pi_\varepsilon\, dA \qquad R = -\int_A E_m\, y\, \pi_\varepsilon\, dA \qquad V = \int_{A_s} G_m\, \pi_\gamma\, dA\,. \tag{19}$$

The upscaling from the micro to the macro structural scale is performed by evaluating the average resultant stress components in the whole UC, as:

$$\begin{aligned} N &= \frac{1}{\ell}\left(\int_{\ell_m} n_m\, dx + \int_{\ell_b} n_b\, dx\right) \\ M &= \frac{1}{\ell}\left(\int_{\ell_m} m_m\, dx + \int_{\ell_b} m_b\, dx\right) \\ T &= \frac{1}{\ell}\left(\int_{\ell_m} t_m\, dx + \int_{\ell_b} t_b\, dx\right). \end{aligned} \tag{20}$$

where ℓ, ℓ_b and ℓ_m are the length of UC, brick and mortar, respectively.

3 Macroscale finite element formulation

A homogeneous Timoshenko beam model is adopted at the macro-level, where the displacement fields are written as:

$$\begin{aligned} U_1 &= U\,(X) - Y\,\Phi\,(X) \\ U_2 &= V\,(X)\ , \end{aligned} \tag{21}$$

with U, V and Φ denoting the beam generalized displacement components, i.e. the axial and transverse displacements of the point (X, Y), and the rotation of the beam cross-section at X, respectively. The counterclockwise rotation is assumed as positive. The beam macroscopic strain components are introduced as:

$$\mathbf{E} = \{E\ K\ \Gamma\}^T\ , \tag{22}$$

with E being the axial elongation, K the curvature and Γ the shear strain. The related macroscopic stress measures read:

$$\mathbf{S} = \{N\ M\ T\}^T\ , \tag{23}$$

where N, M and T are the beam axial, flexural and shear stress components.

To solve the beam structural problem at the macro-level, a 2-node 2D beam FE is formulated adopting the force-based approach and the Gauss-Lobatto integration rule. The element forces

and displacements are expressed in the basic local reference system, obtained by eliminating the rigid body motions, by the following vectors:

$$\mathbf{Q} = \{Q_1\ Q_2\ Q_3\}^T\ ,\ \mathbf{q} = \{q_1\ q_2\ q_3\}^T\ , \tag{24}$$

where Q_1 is the axial force, and Q_2 and Q_3 are the bending moments at the end nodes i and j. Similarly, q_1 is the axial elongation, and q_2 and q_3 are the nodal rotations. The equilibrated stress resultants (23) at each beam cross-section are expressed by the following polynomial interpolation:

$$\mathbf{S} = \mathbf{b}\mathbf{Q} + \mathbf{S}_q\ , \tag{25}$$

with the vector $\mathbf{S}_q = \{N_q\ M_q\ T_q\}^T$ containing the section stresses due to the external loads, distributed along the reference axis. The section equilibrium matrix $\mathbf{b}$ results as:

$$\mathbf{b} = \begin{bmatrix} 1 & 0 & 0 \\ 0 & X/L - 1 & X/L \\ 0 & 1/L & 1/L \end{bmatrix}\ ,$$

L being the length of the beam finite element. The beam strain and stress vectors, $\mathbf{E}$ and $\mathbf{S}$, are related by the section flexibility matrix $\mathbf{f}$. According to the two-scale approach, to determine the constitutive response at each integration point along the beam, the semi-analytical solution of the homogenization problem on the UC is computed [10] and the stress resultants in (20) are derived. The numerical solution of the global incremental nonlinear equilibrium equations follows a classic step-by-step method and a standard iterative Newton-Raphson algorithm.

4 NUMERICAL APPLICATIONS

To validate the proposed two-scale procedure two numerical applications are presented. These consist in the simulation of two masonry structural members subjected to monotonically increasing loads: a rectangular wallette under out-of-plane bending and a circular arch under vertical forces. Both tests are numerically simulated adopting the proposed two-scale model (Two-Scale 1D) compared with two micromechanical approaches (Micro 1D and Micro 2D) and the experimental outcomes.

4.1 Wallette four-point out-of-plane bending test

The first numerical application concerns the four-point out-of-plane bending response of a masonry wallette, experimentally tested in [13]. Figure 2 illustrates the specimen geometry and boundary conditions, and the used 1D discretization. The wallette sizes are: height 675 mm, width 520 mm and thickness 100 mm (Figure 2(a)). The clay brick, having sizes of $T = 100$ mm, $b = 200$ mm and $\ell_b = 50$ mm, are aligned transversally to the flexure plane and the mortar length ℓ_m is equal to 12.5 mm. The top and bottom of the wallette are simply supported at the middle of the outermost brick alignments, and two forces, distributed along the width, act orthogonally to the specimen plane. The distance between the forces is 250 mm. The distance between each force and the nearest support is 187.5 mm.

Accounting for the symmetry of the specimen, the Two-Scale 1D numerical model considers only one half of the wallette, adopting two beam FEs, as illustrated Figure 2(b). Table 1 contains the material model parameters, deduced from the experimental measurements in [13] on the brick and mortar responses. The tensile and shear fracture energies given in [13] as force per unit length have been divided by the area of the three bed mortar joints located in the central beam region, where the moment is constant.

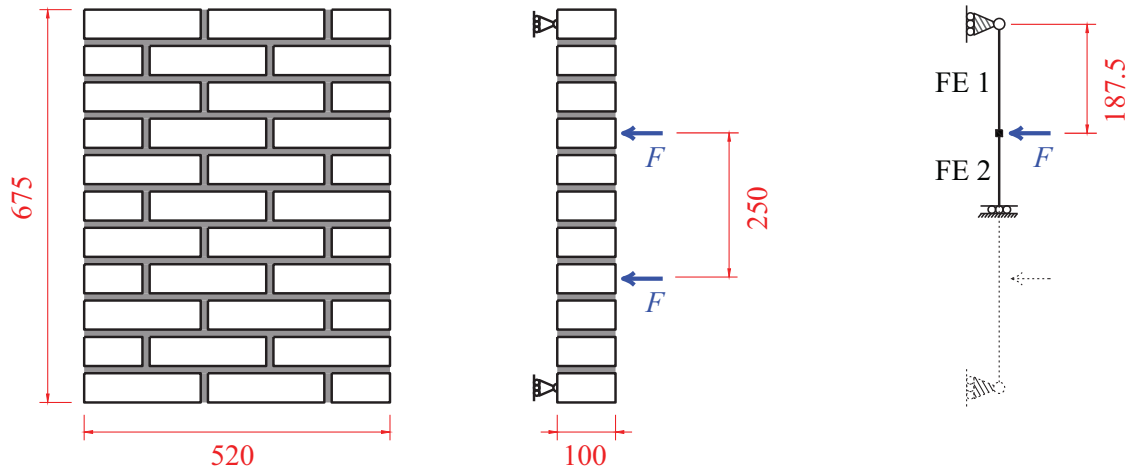

(a) Wallette specimen geometry (b) Two-Scale 1D model configuration

Figure 2: Four-point out-of-plane bending test of the masonry wallette: (a) specimen geometry and (b) macromechanical beam model (dimensions in mm).

Brick			Mortar		
E^b	$=$	16700 MPa	E^m	$=$	5000 MPa
ν^b	$=$	0.13	ν^m	$=$	0.08
			σ_0	$=$	0.4 MPa
			τ_0	$=$	1.9 MPa
			G_{cI}	$=$	1.81×10^{-4} MPa
			G_{cII}	$=$	1.6×10^{-2} MPa
			μ	$=$	0.82

Table 1: Four-point out-of-plane bending test of the masonry wallette: material parameters for the bricks and mortar.

Figure 3 plots the nonlinear response of the wallette in terms of maximum bending moment m per unit width versus the corresponding cross-section curvature K. The numerical results for the Two-Scale 1D model (red line) are compared with the experimental data (blue line) and the results of two micromechanical approaches: a beam FE model (Micro 1D - black dots) and the 2D FE model presented in [7] (Micro 2D - yellow line). The shaded area corresponds to the experimental confidence region, where the upper and lower bound linear-parabola curves have been evaluated by adopting the upper and lower values of the confidence intervals for the parameters, also considered in [14]. The Micro 1D approach discretizes each bed mortar joint and each brick with a homogeneuos beam FE. The Micro 2D approach models the structure in the flexure plane and discretizes the bed mortar joints and the bricks with quadrilateral FEs having uniform thickness. In both models, the FEs representing the bricks behave as linear elastic and those representing the mortar joints adopt the damage-friction constitutive relationship described in Section 2. For the Micro 2D model, the cross-section curvature K is evaluated as the average value occurring in the central region where the moment is constant, following the proposal in [14].

The numerical curves are contained in the confidence area and satisfactorily describe the

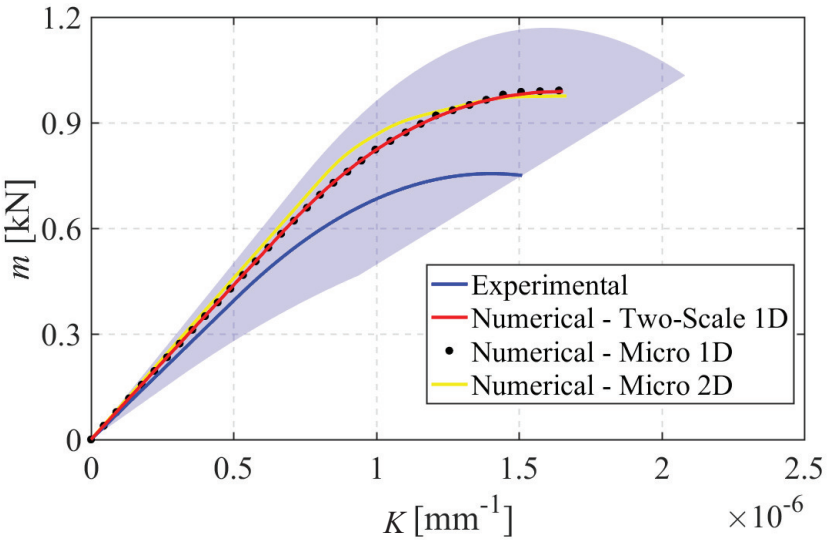

Figure 3: Four-point out-of-plane bending test of the masonry wallette: maximum moment m per unit width versus curvature K.

initial stiffness, the peak strength and the collapse mechanisms of the wallette. Although the experimental maximum strength of the specimen is overestimated, the results for the Two-Scale 1D model fully agree with those of the micromechanical approaches, proving the efficiency of the proposed homogenization procedure. The difference between the numerical and the experimental curves mostly depends on the calibration of the material parameters, whose experimental measurements are affected by considerable uncertainty. Despite this consideration, the proposed numerical procedure results accurate and computationally very fast and efficient.

4.2 Bending of a circular arch

The second numerical application studies the response a masonry circular arch subjected to an eccentric concentrated vertical force. The specimen has been tested during the experimental campaign by Cancelliere et al. [15] and has been numerically studied by Addessi et al. [1]. Figure 4 shows the geometry of the arch, also reporting the conventional numbering of the 23 bricks. The following data are set for the geometry of the specimen: internal radius $r = 456\,\text{mm}$, width $w = 255\,\text{mm}$, thickness $t = 120\,\text{mm}$, height $f = 510\,\text{mm}$ and internal distance between the abutments $d_a = 900\,\text{mm}$. The sizes of the clay bricks are $w = 255\,\text{mm}$, $t = 120\,\text{mm}$ and $\ell_b = 55\,\text{mm}$ and the mortar length varies from $0.8\,\text{mm}$ to $15.5\,\text{mm}$. The vertical force acts on the external surface, at the middle of the 14^{th} brick, that is at the distance $d_f = 140\,\text{mm}$ from the axis of the arch.

Figure 5 shows the discretization adopted for the Two-Scale 1D numerical model. This uses 17 beam FEs, uniformly distributed along the two parts of the arch on the left and right hand sides of the applied force. Table 2 contains the parameters for the material model, deduced from the experimental measurements in [15] on the brick and mortar response and also adopted in [1]. Given the slender geometry of the arch, to reduce the computational burden of the simulations, an Euler-Bernoulli kinematic description of the cross-section is considered, obtained by neglecting the effects of the macroscopic shear strain Γ in the proposed two-scale procedure. Hence, the material parameters for the shear constitutive quantities are not provided. Note that the interface between bricks and mortar joints exhibits a very low tensile resistance during the

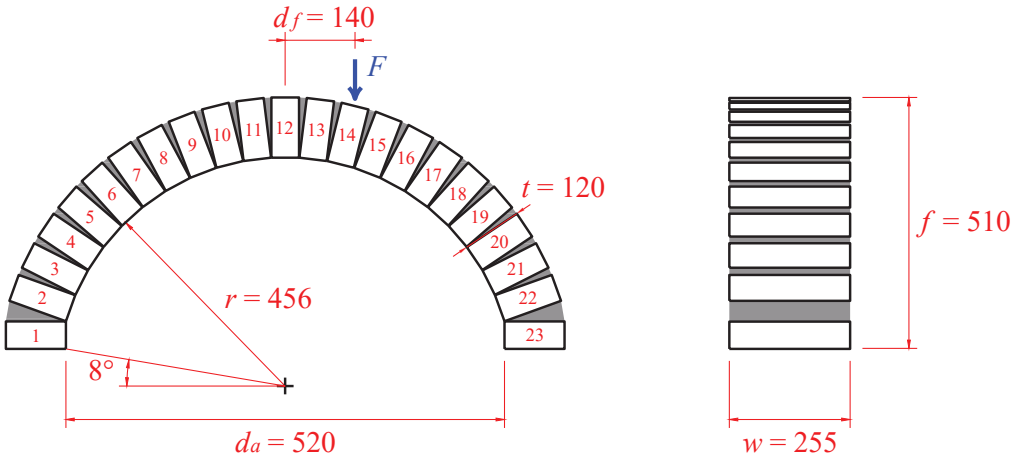

Figure 4: Specimen geometry of the circular arch (dimensions in mm).

experimental test. Hence, a small value of the tensile strength is assumed in the numerical characterization of the mortar. The average value $\ell_m = 10$ mm is assumed for the mortar length and the self weight of the masonry equal to $17\,\mathrm{kN/m^3}$. Moreover, the action of the force is reproduced according to a standard displacement control procedure, that is by restraining the vertical translation of the loaded node and applying an incremental negative displacement v along the vertical direction.

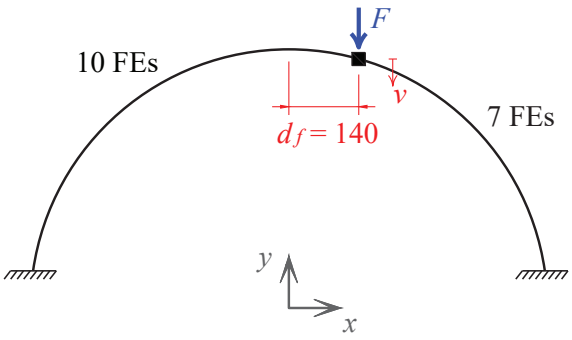

Figure 5: Macromechanical Two-Scale beam model of the circular arch.

Figure 6 plots the nonlinear response of the arch in terms of nodal reaction F versus the prescribed displacement v. The numerical results for the Two-Scale 1D model (red solid line) are compared with the experimental data (blue line) and the results of the Micro 2D approach in [1] (red dotted line). Moreover, the figure indicates the value of the failure load (650 N), deduced by applying the kinematic theorem of the limit analysis. This represents the upper bound of the arch ultimate strength.

The proposed two-scale procedure satisfactorily reproduces the experimental response of the arch and completely agrees with both the experimental and the Micro 2D outcomes. The formation of the hinges leading to the specimen failure is perfectly detected as well. Indeed, four hinges form during the experimental test: two on intrados and two on extrados of the arch, due to the decohesion between the mortar and the brick. These are located as indicated by the red circles in Figure 7(a). In the same figure, the blu dots represent the locations of the hinges

Brick	Mortar
$E^b = 16000$ MPa	$E^m = 1500$ MPa
$\nu^b = 0.20$	$\nu^m = 0.20$
	$\sigma_0 = 1.0 \times 10^{-4}$ MPa
	$G_{cI} = 3.0 \times 10^{-4}$ MPa
	$\mu = 0.50$

Table 2: Material parameters for the bricks and mortar of the circular arch.

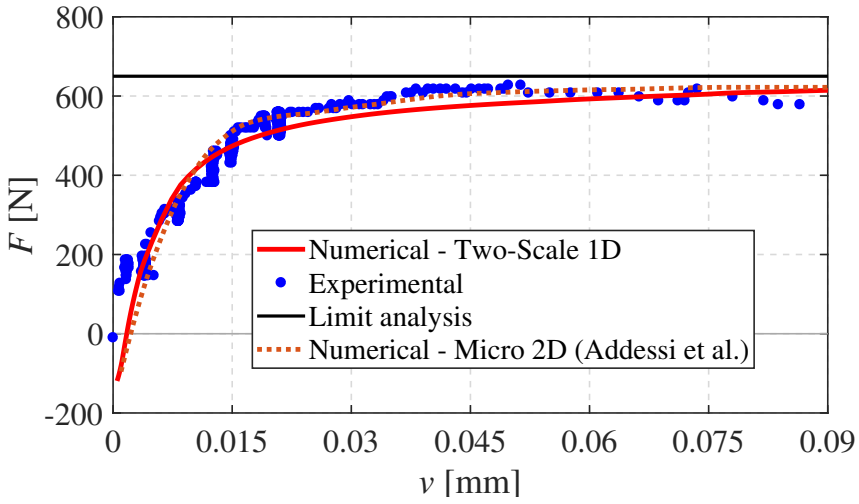

Figure 6: Circular arch: applied force F versus vertical displacement v of the loaded section.

determined by the numerical model. These correspond to the four cross-section with higher values of the damage variable D. The shaded area indicates the average of the damage variable D over each beam cross-section, defined as $D_m = \frac{1}{A}\int_A D\, dA$. For $v = 0.08$ mm, this quantity assumes the values 0.96, 1.00, 1.00 and 0.86 at the hinges, as indicated in the figure. Finally, Figure 7(b) shows the deformed configurations of the arch for the same vertical displacement $v = 0.08$ mm of the loaded cross-section obtained with the Two-Scale 1D model. This accurately matches both the experimental data in [15] and the results of the Micro 2D model in [1] showing a movement of the top of the arch on the left hand side of the force, due to the eccentricity of the load and the formation of the nonlinear hinges.

5 CONCLUSIONS

- Masonry structural elements characterized by geometry and loading conditions typical of beam like structures have been studied.
- A micro-macro two-scale procedure has been employed, using beam FE discretizations at both the structural and UC scale.
- The masonry constituents response has been modeled by a damage-friction plasticity law for the mortar and a linear elastic relationship for the bricks.
- The presented procedure, compared with two micromechanical 1D and 2D FE approaches,

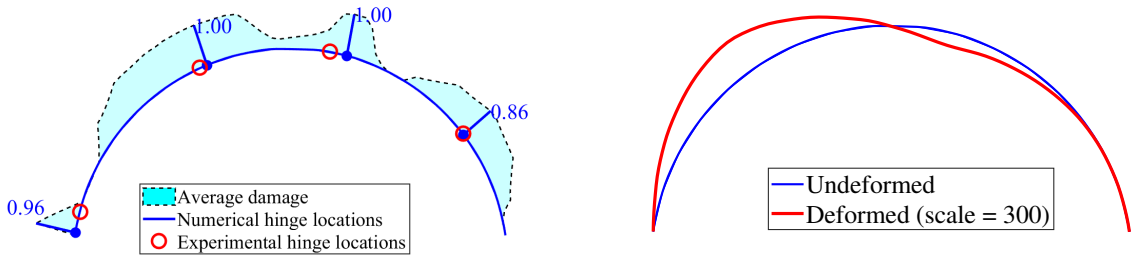

(a) Deformed configuration. (b) Average damage D_m distribution.

Figure 7: Circular arch: (a) deformed configuration and (b) distribution of the average damage D_m and location of the four plastic hinges (blue dots) for $v = 0.8$ mm.

adopting the same constitutive laws for bricks and mortar, is proved to be efficient, fast and accurate.

- The comparison with the experimental outcomes on a masonry wallette under out-of-plane bending and on a vertical loaded circular arch has shown that the two-scale procedure is able to satisfactorily describe the structural response of the analyzed masonry elements and to reproduce the degrading processes involving the mortar joints, as well.

REFERENCES

[1] D. Addessi, S. Marfia, E. Sacco, J. Toti, Modeling Approaches for Masonry Structures. *The Open Civil Engineering Journal*, **8**, 288–300, 2014.

[2] T.J. Massart, R.H.J. Peerlings, M.G.D. Geers, Structural damage analysis of masonry walls using computational homogenization. *International Journal of Damage Mechanics*, **16**, 199–226, 2007.

[3] M.L. De Bellis, D. Addessi, A Cosserat based multi-scale model for masonry structures. *International Journal for Multiscale Computational Engineering*, **9**, 543–563, 2011.

[4] B.C.N. Mercatoris, T.J. Massart, A coupled two-scale computational scheme for the failure of periodic quasi-brittle thin planar shells and its application to masonry. *International Journal for Numerical Methods in Engineering*, **85**, 1177–1206, 2011.

[5] A. Cecchi, K. Sab, A homogenized Love-Kirchhoff model for out-of-plane loaded random 2D lattices: Application to "quasi-periodic" brickwork panels. *International Journal of Solids and Structures*, **46**, 2907–2919, 2009.

[6] M. Petracca, L. Pelà, R. Rossi, S. Oller, G. Camata, E. Spacone, Multiscale computational first order homogenization of thick shells for the analysis of out-of-plane loaded masonry walls. *Computer Methods in Applied Mechanics and Engineering*, **315**, 273–301, 2017.

[7] D. Addessi, E. Sacco, Nonlinear analysis of masonry panels using a kinematic enriched plane state formulation. *International Journal of Solids and Structures*, **90**, 194–214, 2016.

[8] D. Addessi, A. Mastrandrea, E. Sacco, An equilibrated macro-element for nonlinear analysis of masonry structures. *Engineering Structures*, **70**, 82–93, 2014.

[9] R.L. Taylor, *FEAP - A finite element analysis program, Version 8.3*. Department of Civil and Environmental Engineering, University of California at Berkeley, California, 2011.

[10] D. Addessi, E. Sacco, Homogenization of heterogeneous masonry beams. *Meccanica*, https://doi.org/10.1007/s11012-017-0758-2, 2017.

[11] P. Suquet, *Elements of homogenization for inelastic solid mechanics*. Springer-Verlag, Berlin, 1987.

[12] E. Sacco, A nonlinear homogenization procedure for periodic masonry. *European Journal of Mechanics - A/Solids*, **28**, 209–222, 2009.

[13] R. Van der Pluijm, Out-of-plane bending of masonry, behaviour and strength. *PhD Thesis, Eindhoven University of Technology*, The Netherlands, 1999.

[14] R. Serpieri, M. Albarella, E. Sacco, A 3D microstructured cohesive-frictional interface model and its rational calibration for the analysis of masonry panels. *International Journal of Solids and Structures*, https://doi.org/10.1016/j.ijsolstr.2017.06.006, 2017.

[15] I. Cancelliere, M. Imbimbo, E. Sacco, Experimental tests and numerical modeling of reinforced masonry arches. *Engineering Structures*, **32**, 776–792, 2010.